

# Substructuring-based dynamic reduction method for vibration analysis of periodic composite structures

Robel Weldebrhan Hagos<sup>1</sup>, Geomji Choi<sup>1</sup>, Heejun Sung<sup>2</sup> and Seongmin Chang<sup>\*1,3</sup>

<sup>1</sup>Department of Mechanical Engineering, Kumoh National Institute of Technology,  
Daehak-ro 61, Gumi, Gyeongbuk 39177, Korea

<sup>2</sup>Multiscale Mechanical Design Division, School of Mechanical and Aerospace Engineering,  
Seoul National University, 1 Gwanak-ro, Seoul 08826, Korea

<sup>3</sup>Department of Mechanical Design Engineering, Kumoh National Institute of Technology,  
Daehak-ro 61, Gumi, Gyeongbuk 39177, Korea

(Received January 12, 2022, Revised February 19, 2022, Accepted March 5, 2022)

**Abstract.** Macro periodic composite structures are often represented by large-scale finite element (FE) models, so conventional FE methods and component mode synthesis (CMS) techniques are inadequate for assessing the dynamics of these structures in a reasonable amount of time. This study proposes the improved reduction system (IRS) combined with a substructuring scheme for modal analysis of periodic composite structures; and compares it with the homogenization method. Model reduction and homogenization are performed utilizing in-house code and ANSYS®, respectively. In IRS-based substructuring, the macrostructure is subdivided into identical substructures, then a single representative volume element (RVE) is taken and reduced. The reduced substructures are assembled into a macrostructure with fewer degrees of freedom (DOFs), resulting in an accurate and efficient result with a small memory footprint. According to our findings, the proposed method provides accurate results independent of the number of substructures contained within the macrostructure, whereas the homogenization method relies on the number of substructures present.

**Keywords:** homogenization; IRS; periodic composite structures; RVE; substructuring

## 1. Introduction

Periodic structures are made up of repetitive unit cells arranged in a continuous form. They are designed for aesthetics, manufacturing, and functionality and have various applications in modern structures, including additive manufacturing and lattice structures. To achieve multi-functionality, they can be extended to functionally graded structures. Periodic composite materials are made by layering or otherwise integrating two or more different kinds of materials to form a new material with a distinct set of properties. As a result, they combine the most desirable properties of their component materials resulting in a product that is both light and strong (Benjeddou and Guerich 2019, Antony *et al.* 2019, Rachedi *et al.* 2020, Sayyad and Ghugal 2020, Pourmoayed *et al.* 2021). In finite element analysis, modeling composite materials often involve performing experimental tests to determine the exact material properties. These tests can be time and resource-consuming.

---

\*Corresponding author, Assistant Professor, E-mail: schang@kumoh.ac.kr

Composite structures are also difficult to simulate numerically due to the different length scales involved. Benjeddou and Guerich (2019) proposed a FE approach for free vibration analysis of aircraft and spacecraft hexagonal honeycomb sandwich panels, and they pointed out that detailed FE approaches for simulating honeycomb sandwich structures had rarely been investigated because the computational effort associated with them rapidly increases as the number of core cells increases. There are times when the composite structure is too long in comparison to the component materials. Even though the structural mechanics of these systems can be computed using the finite element method (resolving all length scales), it is not practical because the number of elements required would be astronomically large. As a result, analysis methods have attempted to approximate composites' mechanical behavior through analyzing a representative volume element (RVE) of the composite microstructure. Hill (1963) introduced the term RVE in 1963, noting that the RVE was structurally typical of composite materials and contained enough inclusions to ensure the apparent moduli were independent of RVE boundary displacements. Additionally, Hashin (1983) demonstrated that stress and strain fields in the RVE are homogeneous when homogeneous boundary conditions are given except for a layer near the external surface (Hollister and Kikuchi 1992).

The RVE method separates the analysis of composite materials into local and global analyses. Using the local level analysis, the microstructural details are modeled to determine effective elastic properties. In addition, the relationship between the local strain within the RVE and the effective or average RVE strain is calculated. The composite structure is then replaced with an equivalent homogeneous material with the calculated effective properties. In the global level analysis, the effective stress and strain are calculated within the homogeneous equivalent structure. The process of computing effective properties has been termed "homogenization" by Suquet (1987). Using homogenized material data structures only need to be simulated at the macroscopic level, making composite simulation significantly less computationally expensive. It is possible to obtain estimates of local stresses and strains by using the relationship between the average and local strain from the local analysis, and this procedure is called "localization" (Suquet 1987) or dehomogenization (Hollister and Kikuchi 1992).

As structures and mechanical systems become complex, they require sophisticated simulation techniques for design, control, and optimization. In finite element analysis (FEA), the computational effort is approximately proportional to the cubic of the problem size (Qu 2004); if the problem size is reduced, the computational work could be reduced significantly. Thus, several techniques have been proposed to reduce the size of large models before they are analyzed in detail. Examples include component mode synthesis, dynamic condensation, dynamic substructuring, and the Ritz vector approach. Through the application of a model reduction technique, the size of a full model can be significantly reduced. However, the reduced model does not retain all features of the full model because of the truncated errors. Even though most reduction techniques aim to keep the key features within a certain frequency range, this may not be exactly the case. Consequently, there exists a trade-off between model size and accuracy. Model reduction is all about trying to get the smallest model that contains the most information out of the full model.

Dynamic condensation was proposed in 1965 as an efficient method for model reduction. According to this technique, there are master and slave degrees of freedom for a given value of the system's degrees of freedom. As a result, the dynamic condensation matrix defines the relationship between the responses or mode shapes between the master and slave degrees of freedom. Through dynamic condensation, the system matrices of a full model can be reduced to the dimensions of just the master degrees of freedom. Unlike other model reduction techniques, the reduced model from

dynamic condensation is defined in a subspace of the full displacement space and each coordinate has its physical meaning.

Dynamic substructuring (DS) is the decomposition of a complex dynamic system into smaller parts called substructure (Klerk *et al.* 2008). DS is best understood as a framework for synthesizing components rather than a method of its own (Seijs 2016). Often, the idea is related to the mathematical concept of domain decomposition by Schwarz (Schwarz 1890) or the ancient principle of “divide and conquer”. DS was first introduced in the 1960s to solve large FEM models that were not manageable with computing resources available at that time. It is possible to solve smaller substructures individually and synthesize them by satisfying coordinate compatibility and force equilibrium at the substructure’s interface (Craig Jr. and Bampton 1968, Hurty 1960, Rixen 2004).

As micromechanical FEA is increasingly used for the characterization of modern composite materials with sophisticated microstructures (Li 2008, Li *et al.* 2015), this study presents an improved reduced system (IRS) method (O’Callahan 1989) for vibration analysis of periodic composite structures. The proposed method has the following merits: first, it applies the IRS method, which diminishes the eigenvalue error reduction significantly by accounting for the effect of inertia terms of the slave DOFs. Second, it employs a substructuring scheme, which requires less computing time and memory usage for the construction of the reduced system, even when the problem has a large number of degrees of freedom.

The paper is organized as follows: Section 2 presents an overview of the homogenization theory. Section 3 discusses model order reduction and substructuring for periodic structures in detail. Section 4 describes the computational procedure for the proposed method, and Section 5 presents a numerical example and compares the modal analysis results of the proposed and homogenization methods.

## 2. Review of homogenization theory

Based on the details presented by Bendsøe and Kikuchi (1988), Guedes and Kikuchi (1990), and Cho *et al.* (2011), this section discusses the basic formulation of the homogenization method. According to homogenization theory, it is generally assumed that composite material is locally formed by repeated discrete microstructures, such as ‘microscopic’ cells, compared to the overall size of the structure of interest on a macroscopic scale. Accordingly, the microscopic variable is assumed to determine material properties periodically, where the period is smaller than the macroscopic variable. Based on this assumption, equivalent material properties can be determined by reducing microscopic cell sizes to zero (Guedes and Kikuchi 1990). The overall macroscopic domain in composites with size-dependent elastic moduli is composed of microscopic periodic base cells, as shown in Fig. 1. Macroscopically,  $V^\varepsilon$  is the matrix domain. The boundary,  $S^0$ , is divided into two parts; traction  $S_1^0$  and displacement  $S_2^0$ .

$S_1^0$  and  $S_2^0$  are stipulated as follows

$$\mathbf{u} = \bar{\mathbf{u}} \text{ on } S_1^0, \quad \mathbf{t} = \bar{\mathbf{t}} \text{ on } S_2^0 \quad (1)$$

Along with the macroscopic domain boundary  $S^h$ , the effective interface boundaries can be defined as  $S^{hi}$ . The formulation assumes no external force acts on the boundary,  $S^{hi}$ . Due to the heterogeneity that repeats within the macroscopic domain, it makes sense to separate the microscopic behavior of composites from the macroscopic behavior when subjected to external loads and prescribed displacements. Hence, the macroscopic and microscopic coordinate systems,  $X$  and  $y$ , respectively, can be defined as follows

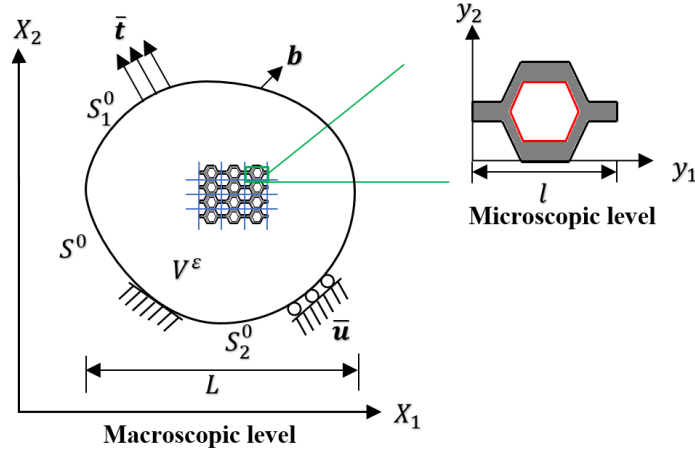


Fig. 1 Micro and macro structures of periodic composite in domain  $V^\varepsilon$ , with traction and displacement boundary conditions, indicated by  $S_1^0$  and  $S_2^0$ , respectively

$$\mathbf{X} = \mathbf{X}(\mathbf{x}, \mathbf{y}), \quad \mathbf{x} = \mathbf{X}, \quad \mathbf{y} = \mathbf{X}/\varepsilon \quad (2)$$

where  $\varepsilon$  describes the ratio of macro to microscale as a non-dimensional parameter, which is given as

$$\varepsilon = \frac{1}{L}, \quad 0 < \varepsilon = \frac{1}{L} < 1 \quad (3)$$

The virtual work can be expressed as a strong form of the real displacement field,  $\mathbf{u}$ , and the virtual displacement,  $\mathbf{v}$ , as shown in Eq. (4) when a body force,  $\mathbf{b}$ , is applied to the matrix domain and traction,  $\bar{\mathbf{t}}$ , on the boundary,  $S_2^0$ .

$$\int_{V^\varepsilon} \nabla_X \mathbf{u} : \mathbf{C} : \nabla_X \mathbf{v} dV_X = \int_{V^\varepsilon} \mathbf{b} \cdot \mathbf{v} dV_X + \int_{S_2^0} \bar{\mathbf{t}} \cdot \mathbf{v} dS_X \quad (4)$$

where  $\mathbf{C}$  is the fourth-order stiffness tensor ( $C_{ijkl}$ ). A macroscale, as well as microscale behavior, can be described using Eq. (5), which expresses the displacement field,  $\mathbf{u}$ , as an asymptotic form of the parameter,  $\varepsilon$ .

$$\mathbf{u}(X) = \mathbf{u}^0(\mathbf{x}, \mathbf{y}) + \varepsilon \mathbf{u}^1(\mathbf{x}, \mathbf{y}) + \varepsilon^2 \mathbf{u}^2(\mathbf{x}, \mathbf{y}) + \dots \quad (5)$$

Since the virtual displacement,  $\mathbf{v}$ , is an arbitrary function that can be defined as a function of  $\mathbf{x}$  and  $\mathbf{y}$  as follows

$$\mathbf{v}(X) = \mathbf{v}(\mathbf{x}, \mathbf{y}) \quad (6)$$

Using partial derivatives of the displacement fields based on the two coordinate systems, Eqs. (5)-(6) can be written as

$$\frac{\partial \Psi(\mathbf{x}, \mathbf{y})}{\partial x_i} = \frac{\partial \Psi}{\partial x_i} + \frac{1}{\varepsilon} \frac{\partial \Psi}{\partial y_i}, \quad \Psi(\mathbf{x}, \mathbf{y}) = \mathbf{u}(\mathbf{x}, \mathbf{y}) \text{ or } \mathbf{v}(\mathbf{x}, \mathbf{y}) \quad (7)$$

If  $\varepsilon$  is sufficiently small ( $\varepsilon \rightarrow 0$ ), then the volume and surface integral of a function,  $\Phi(\mathbf{X})$ , in the macroscopic domain,  $\mathbf{X}$ , can be transformed as follows

*Substructuring-based dynamic reduction method for vibration analysis of periodic composite structures*

$$\begin{aligned}\lim_{\varepsilon \rightarrow 0} \int_{V^\varepsilon} \Phi(\mathbf{X}) dV_x &= \int_V \frac{1}{\text{vol}(V_x^C)} \left[ \int_{V^C} \Phi(\mathbf{x}, \mathbf{y}) \varepsilon^3 dV_y \right] dV_x \\ &= \int_V \frac{1}{\text{vol}(V_y^C)} \left[ \int_{V_y^C} \Phi(\mathbf{x}, \mathbf{y}) dV_y \right] dV_x\end{aligned}\quad (8)$$

$$\begin{aligned}\lim_{\varepsilon \rightarrow 0} \int_{V^\varepsilon} \Phi(\mathbf{X}) dS_x &= \int_V \frac{1}{\text{vol}(V_x^C)} \left[ \int_{S^{hi}} \Phi(\mathbf{x}, \mathbf{y}) \varepsilon^2 dS_y \right] dV_x \\ &= \frac{1}{\varepsilon} \int_V \frac{1}{\text{vol}(V_y^C)} \left[ \int_{S^{hi}} \Phi(\mathbf{x}, \mathbf{y}) dS_y \right] dV_x\end{aligned}$$

where volumes  $V$  and  $V^C$  represent the homogenized macroscopic and unit cell domains, respectively. Eqs. (9)-(11) are obtained by introducing Eq. (5) into Eq. (4), applying Eqs. (7)-(8), and arranging the terms referring to  $\varepsilon$ .

$$o\left(\frac{1}{\varepsilon^2}\right): \int_V \frac{1}{\text{vol}(V_y^C)} \left[ \int_{V_y^C} \nabla_y \mathbf{u}^0 : \mathbf{C} : \nabla_y \mathbf{v} dV_y \right] dV_x = 0 \quad (9)$$

$$o\left(\frac{1}{\varepsilon}\right): \int_V \frac{1}{\text{vol}(V_y^C)} \left[ \int_{V_y^C} \nabla_y \mathbf{u}^0 : \mathbf{C} : \nabla_x \mathbf{v} + (\nabla_x \mathbf{u}^0 + \nabla_y \mathbf{u}^1) : \mathbf{C} : \nabla_y \mathbf{v} \right] dV_y dV_x = 0 \quad (10)$$

$$\begin{aligned}(1): \int_V \frac{1}{\text{vol}(V_y^C)} \left[ \int_{V_y^C} (\nabla_x \mathbf{u}^0 + \nabla_y \mathbf{u}^1) : \mathbf{C} : \nabla_x \mathbf{v} + (\nabla_x \mathbf{u}^1 + \nabla_x \mathbf{u}^2) : \mathbf{C} : \nabla_y \mathbf{v} \right] dV_y dV_x \\ = \int_V \frac{1}{\text{vol}(V_y^C)} \int_{V_y^C} \mathbf{b} \cdot \mathbf{v} dV_y dV_x + \int_{S^0} \bar{\mathbf{t}} \cdot \mathbf{v} dS_x\end{aligned}\quad (11)$$

Sequentially solving Eqs. (9)-(11) yields the displacement field,  $\mathbf{u}(\mathbf{x}, \mathbf{y})$ . Applying the divergence theorem and accounting for  $\mathbf{v}(\mathbf{x}, \mathbf{y})$  is arbitrary,  $\mathbf{u}^0(\mathbf{x}, \mathbf{y})$  is obtained from Eq. (9) as a function of  $\mathbf{x}$ .

$$\mathbf{u}^0(\mathbf{x}, \mathbf{y}) = \mathbf{u}^0(\mathbf{x}) \quad (12)$$

To find the differential equations stated below, first, we incorporate Eq. (12) into Eq. (10) and then assume that the virtual displacement represents an arbitrary function of  $\mathbf{y}$ , viz.,  $\mathbf{v}(\mathbf{y})$ , and finally apply the divergence theorem to Eq. (10).

$$-\nabla_y \cdot [\mathbf{C} : \nabla_y \mathbf{u}^1] = -\nabla_y \cdot [\mathbf{C} : \nabla_x \mathbf{u}^0] \quad (13)$$

$$\mathbf{n} \cdot [\mathbf{C} : (\nabla_y \mathbf{u}^1)] = -\mathbf{n} \cdot [\mathbf{C} : (\nabla_x \mathbf{u}^0)] \quad (14)$$

Based on Eqs. (13)-(14), the displacement field,  $\mathbf{u}^1(\mathbf{x}, \mathbf{y})$ , is correlated with the displacement field,  $\mathbf{u}^0(\mathbf{x})$ , as follows

$$\mathbf{u}^1(\mathbf{x}, \mathbf{y}) = -\boldsymbol{\chi}(\mathbf{x}, \mathbf{y}) : \nabla_x \mathbf{u}^0(\mathbf{x}) \text{ or } (u_i^1 = -\chi_{ijk} u_{j,k}^0) \quad (15)$$

where  $\boldsymbol{\chi}(\mathbf{x}, \mathbf{y})$  is a third-order tensor describing the behavior of the base-cell. The weak form of

Eqs. (13)-(14) related to the third-order tensor,  $\boldsymbol{\chi}(\mathbf{x}, \mathbf{y})$ , can be obtained by inserting Eq. (15) into Eqs. (13)-(14), and recalling that  $\nabla_x \mathbf{u}^0(\mathbf{x})$  is a function of  $\mathbf{x}$ .

$$\int_{V_y^c} \nabla_y \mathbf{v}(\mathbf{y}) : \mathbf{C} : \nabla_y \boldsymbol{\chi} dV_y = \int_{V_y^c} \nabla_y \mathbf{v}(\mathbf{y}) : \mathbf{C} dV_y \quad (16)$$

To obtain the homogenized elastic modulus with the singular perturbation method, we must then take Eq. (11) and calculate the macroscopic equilibrium condition. Selecting the virtual displacement based on,  $\mathbf{x}$ , viz.,  $\mathbf{v}(\mathbf{y})$ , we can obtain

$$\begin{aligned} & \int_V \frac{1}{\text{vol}(V_y^c)} \left[ \int_{V_y^c} (\nabla_x \mathbf{u}^0 + \nabla_y \mathbf{u}^1) : \mathbf{C} : dV_y \right] \nabla_x \mathbf{u} dV_x \\ &= \int_V \frac{1}{\text{vol}(V_y^c)} \int_{V_y^c} (\mathbf{b} dV_y) \cdot \mathbf{v}(\mathbf{x}) dV_x + \int_{S_0} \bar{\mathbf{t}} \cdot \mathbf{u} dS_x \end{aligned} \quad (17)$$

By substituting Eq. (15) for  $\mathbf{u}^1(\mathbf{x}, \mathbf{y})$ , we obtain the macroscopic equilibrium equation containing the homogenized elastic modulus tensor as

$$\int_V \nabla_x \mathbf{v}(\mathbf{x}) : \mathbf{C}_H : \nabla_x \mathbf{u}^0(\mathbf{x}) dV_x = \int_{S_0} \mathbf{v}(\mathbf{x}) \cdot \bar{\mathbf{t}} dS_x \quad (18)$$

where  $\mathbf{C}_H$  is the homogenized fourth-order elastic stiffness tensor and is given by

$$\mathbf{C}_H = \frac{1}{\text{vol}(V_y^c)} \int_{V_y^c} (\mathbf{C} - \mathbf{C} : \nabla_y \boldsymbol{\chi}) dV_y \quad (19)$$

Eq. (16) should be numerically solved to obtain the tensor,  $\boldsymbol{\chi}(\mathbf{x}, \mathbf{y})$ , to calculate the homogenized elastic stiffness.

### 3. Model order reduction and substructuring

#### 3.1 Model order reduction-General concepts

The Finite Element Method (FEM) is a common spatial discretization method when it comes to mechanical multi-degree-of-freedom (multi-DOF) systems. An  $n$  – DOFs system's dynamic equilibrium can be expressed in matrix form as

$$\mathbf{M} \ddot{\mathbf{x}}(t) + \mathbf{C} \dot{\mathbf{x}}(t) + \mathbf{K} \mathbf{x}(t) = \mathbf{F}(t) \quad (20)$$

where  $\mathbf{M}, \mathbf{C}, \mathbf{K} \in \mathbb{R}^{n \times n}$  represent the linearized system matrices for mass, damping, and stiffness, respectively.  $\mathbf{x} \in \mathbb{R}^{n \times 1}$  is the set of displacements for all  $n$  degrees of freedom and  $\mathbf{F}(t) \in \mathbb{R}^{n \times 1}$  is the load vector.

Physical displacements in the time domain (discretized at nodes) are expressed by the unknown  $\mathbf{x}$  in Eq. (20). As a general principle, model reduction consists of finding a low dimension subspace  $\mathbf{T} \in \mathbb{R}^{n \times m}$  with  $m \ll n$  to approximate the state vector  $\mathbf{x}$ , i.e.,  $\mathbf{x} = \mathbf{T} \mathbf{x}_R + \boldsymbol{\varepsilon}$ . A linear 2nd-order ODE of lower dimension can be derived by projecting Eq. (20) on that subspace.

$$\mathbf{M}_R \ddot{\mathbf{x}}_R(t) + \mathbf{C}_R \dot{\mathbf{x}}_R(t) + \mathbf{K}_R \mathbf{x}_R(t) = \mathbf{F}_R \quad (21)$$

*Substructuring-based dynamic reduction method for vibration analysis of periodic composite structures*

where  $\mathbf{M}_R = \mathbf{T}^T \mathbf{M} \mathbf{T}$ ,  $\mathbf{C}_R = \mathbf{T}^T \mathbf{C} \mathbf{T}$ ,  $\mathbf{K}_R = \mathbf{T}^T \mathbf{K} \mathbf{T}$  are the reduced system matrices with dimension  $\mathbb{R}^{m \times m}$  and  $\mathbf{F}_R = \mathbf{T}^T \mathbf{F}$  is the reduced load vector of dimension  $\mathbb{R}^{m \times 1}$ . The effectiveness and reliability of the reduction depend on the size of  $\varepsilon$ . Over the past decades, various techniques have been developed that have some characteristics in common depending on the choice of  $\mathbf{T}$  (Benner 2006, Koutsovasilis and Beitelshmidt 2008).

Some of the model order reduction techniques include Guyan-Irons reduction (Guyan 1965, Irons 1965), dynamic reduction (Miller 1980), improved reduction system (IRS), and its iterative variant (O'Callahan 1989, Blair *et al.* 1991, Friswell *et al.* 1995), component mode synthesis (CMS) (Craig Jr. and Bampton 1968, C. Hurty 1960), and system equivalent expansion and reduction process (SEREP) (O'Callahan *et al.* 1988, Kammer 1987). The Guyan-Irons reduction and IRS method are discussed in this paper, but first, we need to partition the system matrices in Eq. (20) into sub-blocks, as master/external ( $m$ ) and slave/internal ( $s$ ) DOFs

$$\begin{aligned} \tilde{\mathbf{M}} \ddot{\tilde{\mathbf{x}}}(t) + \tilde{\mathbf{C}} \dot{\tilde{\mathbf{x}}}(t) + \tilde{\mathbf{K}} \tilde{\mathbf{x}}(t) &= \tilde{\mathbf{F}} \\ \tilde{\square} &:= \begin{pmatrix} [\square]_{mm} & [\square]_{ms} \\ [\square]_{sm} & [\square]_{ss} \end{pmatrix}, \quad [\square] = \{\mathbf{M}, \mathbf{C}, \mathbf{K}\} \\ \tilde{\mathbf{x}} &:= \begin{pmatrix} \mathbf{x}_m \\ \mathbf{x}_s \end{pmatrix}, \quad \tilde{\mathbf{F}} := \begin{pmatrix} \mathbf{F}_m \\ \mathbf{F}_s \end{pmatrix} \\ m \cup s &= n, \quad n = \text{DOF}_{\text{total}}, \quad m \cap s = \emptyset \end{aligned} \quad (22)$$

### 3.1.1 Guyan-Irons reduction

Guyan (1965) and Irons (1965) proposed a common method of finding a reasonably accurate representation space,  $\mathbf{T}$ . The internal DOFs are assumed to be force-free, i.e.,  $\mathbf{F}_s = 0$ , and assuming undamped system Eq. (22) is solved for  $\mathbf{x}_s$ . The transformation matrix for the static reduction, Eq. (25), is obtained by omitting the equivalent inertia terms in Eq. (24). In this case,  $\mathbf{T}_G$  represents the low dimension subspace.

$$\mathbf{x}_s = -\mathbf{K}_{ss}^{-1} (\mathbf{M}_{sm} \ddot{\mathbf{x}}_m + \mathbf{M}_{ss} \ddot{\mathbf{x}}_s + \mathbf{K}_{sm} \mathbf{x}_m) \quad (23)$$

$$\mathbf{M}_{sm} \ddot{\mathbf{x}}_m + \mathbf{M}_{ss} \ddot{\mathbf{x}}_s = \mathbf{0} \quad (24)$$

$$\begin{pmatrix} \mathbf{x}_m \\ \mathbf{x}_s \end{pmatrix} = \begin{pmatrix} \mathbf{I} \\ -\mathbf{K}_{ss}^{-1} \mathbf{K}_{sm} \end{pmatrix} \cdot \mathbf{x}_m = \mathbf{T}_G \cdot \mathbf{x}_m \quad (25)$$

$$\mathbf{T}_G = \begin{pmatrix} \mathbf{I} \\ -\mathbf{K}_{ss}^{-1} \mathbf{K}_{sm} \end{pmatrix} \quad (26)$$

Using  $\mathbf{T}_G$  the reduced stiffness and mass matrices become

$$\begin{aligned} \mathbf{K}_G &= \mathbf{T}_G^T \mathbf{K} \mathbf{T}_G = \mathbf{K}_{mm} - \mathbf{K}_{ms} \mathbf{K}_{ss}^{-1} \mathbf{K}_{sm} \\ \mathbf{M}_G &= \mathbf{T}_G^T \mathbf{M} \mathbf{T}_G = \mathbf{M}_{mm} - \mathbf{M}_{ms} \mathbf{K}_{ss}^{-1} \mathbf{K}_{sm} - \mathbf{K}_{ms} \mathbf{K}_{ss}^{-1} \mathbf{M}_{sm} + \mathbf{K}_{ms} \mathbf{K}_{ss}^{-1} \mathbf{M}_{ss} \mathbf{K}_{ss}^{-1} \mathbf{K}_{sm} \end{aligned} \quad (27)$$

In general, Guyan-Irons reduction provides a good approximation for smaller eigenvalues and eigenvectors. For high-frequency motion, however, Inertia terms become significant, which makes this method inaccurate.

### 3.1.2 Improved Reduction System (IRS) method

The IRS method is what O'Callaghan (1989) proposed as a modified method. By taking inertia terms into account as pseudo-static forces, the IRS perturbs the static transformation. The free vibration of the undamped reduced system, Eq. (21), gives

$$\mathbf{M}_R \ddot{\mathbf{x}}_m + \mathbf{K}_R \mathbf{x}_m = \mathbf{0} \Rightarrow \ddot{\mathbf{x}}_m = -\mathbf{M}_R^{-1} \mathbf{K}_R \mathbf{x}_m \quad (28)$$

where  $\mathbf{K}_R$  and  $\mathbf{M}_R$  are reduced stiffness and mass matrices obtained from Guyan-Irons reduction, and we can replace them with  $\mathbf{K}_G$  and  $\mathbf{M}_G$ , respectively. By differentiating Eq. (25)

$$\ddot{\mathbf{x}}_s = -\mathbf{K}_{ss}^{-1} \mathbf{K}_{sm} \ddot{\mathbf{x}}_m \quad (29)$$

By substituting Eq. (28) into Eq. (29), we get Eq. (30).

$$\ddot{\mathbf{x}}_s = \mathbf{K}_{ss}^{-1} \mathbf{K}_{sm} \mathbf{M}_G^{-1} \mathbf{K}_G \mathbf{x}_m \quad (30)$$

Eqs. (28)-(30) are substituted into Eq. (23), resulting in the IRS transformation matrix as follows

$$\mathbf{x}_s = [-\mathbf{K}_{ss}^{-1} \mathbf{K}_{sm} + \mathbf{K}_{ss}^{-1} \mathbf{S} \mathbf{M}_G^{-1} \mathbf{K}_G] \mathbf{x}_m \quad (31)$$

$$\mathbf{S} = \mathbf{M}_{sm} - \mathbf{M}_{ss} \mathbf{K}_{ss}^{-1} \mathbf{K}_{sm}$$

$$\begin{pmatrix} \mathbf{x}_m \\ \mathbf{x}_s \end{pmatrix} = \mathbf{T}_{IRS} \cdot \mathbf{x}_m, \mathbf{P} = \begin{pmatrix} \mathbf{0} & \mathbf{0} \\ \mathbf{0} & \mathbf{K}_{ss}^{-1} \end{pmatrix} \quad (32)$$

$$\mathbf{T}_{IRS} = \mathbf{T}_G + \mathbf{P} \mathbf{M}_G^{-1} \mathbf{K}_G \quad (33)$$

$\mathbf{T}_{IRS}$  is dependent on the reduced stiffness and mass matrices obtained from the static reduction. The reduced stiffness and mass matrices of the IRS method are given as follows

$$\begin{aligned} \mathbf{K}_{IRS} &= \mathbf{T}_{IRS}^T \mathbf{K} \mathbf{T}_{IRS} = \mathbf{K}_{mm} + \mathbf{K}_{ms} \mathbf{T}_{IRS} + \mathbf{T}_{IRS}^T \mathbf{K}_{sm} + \mathbf{T}_{IRS}^T \mathbf{K}_{ss} \mathbf{T}_{IRS} \\ \mathbf{M}_{IRS} &= \mathbf{T}_{IRS}^T \mathbf{M} \mathbf{T}_{IRS} = \mathbf{M}_{mm} + \mathbf{M}_{ms} \mathbf{T}_{IRS} + \mathbf{T}_{IRS}^T \mathbf{M}_{sm} + \mathbf{T}_{IRS}^T \mathbf{M}_{ss} \mathbf{T}_{IRS} \end{aligned} \quad (34)$$

### 3.2 Substructuring using the IRS method

Substructuring requires splitting up the whole structure into smaller pieces. Based on the paper by Choi *et al.* (2008), we present the derivation of the basic substructuring reduction procedure using the IRS method. Assuming an undamped system, the eigenvalue problem of Eq. (20) is

$$\mathbf{K} \Phi = \mathbf{M} \Phi \Lambda \quad (35)$$

where  $\Phi$  represents the vibrating mode (eigenvector), corresponding to eigenvalue  $\Lambda$ .

To develop the basic substructuring formulation, the entire system is divided into two substructures, in which the system matrices are constructed independently. In the case of substructure one, the eigenvalue problem can be expressed as follows

$$\begin{bmatrix} \mathbf{K}_{ss}^{(1)} & \mathbf{K}_{sm}^{(1)} \\ \mathbf{K}_{ms}^{(1)} & \mathbf{K}_{mm}^{(1)} \end{bmatrix} \begin{bmatrix} \Phi_{sm}^{(1)} \\ \Phi_{mm}^{(1)} \end{bmatrix} = \begin{bmatrix} \mathbf{M}_{ss}^{(1)} & \mathbf{M}_{sm}^{(1)} \\ \mathbf{M}_{ms}^{(1)} & \mathbf{M}_{mm}^{(1)} \end{bmatrix} \begin{bmatrix} \Phi_{sm}^{(1)} \\ \Phi_{mm}^{(1)} \end{bmatrix} \Lambda_{mm} \quad (36a)$$

As for substructure two, the eigenvalue problem can be described separately as follows

$$\begin{bmatrix} \mathbf{K}_{mm}^{(2)} & \mathbf{K}_{ms}^{(2)} \\ \mathbf{K}_{sm}^{(2)} & \mathbf{K}_{ss}^{(2)} \end{bmatrix} \begin{bmatrix} \Phi_{mm}^{(2)} \\ \Phi_{sm}^{(2)} \end{bmatrix} = \begin{bmatrix} \mathbf{M}_{mm}^{(2)} & \mathbf{M}_{ms}^{(2)} \\ \mathbf{M}_{sm}^{(2)} & \mathbf{M}_{ss}^{(2)} \end{bmatrix} \begin{bmatrix} \Phi_{mm}^{(2)} \\ \Phi_{sm}^{(2)} \end{bmatrix} \Lambda_{mm} \quad (36b)$$



*Substructuring-based dynamic reduction method for vibration analysis of periodic composite structures*

A global system can be constructed by combining stiffness matrices and mass matrices, as shown in Eq. (37).

$$\begin{bmatrix} \mathbf{K}_{ss}^{(1)} & \mathbf{K}_{sm}^{(1)} \\ \mathbf{K}_{ms}^{(1)} & \mathbf{K}_{mm}^{(1)} & \mathbf{K}_{ms}^{(2)} \\ & \mathbf{K}_{sm}^{(2)} & \mathbf{K}_{ss}^{(2)} \end{bmatrix} \begin{bmatrix} \Phi_{sm}^{(1)} \\ \Phi_{mm}^{(1)} \\ \Phi_{sm}^{(2)} \end{bmatrix} = \begin{bmatrix} \mathbf{M}_{ss}^{(1)} & \mathbf{M}_{sm}^{(1)} \\ \mathbf{M}_{ms}^{(1)} & \mathbf{M}_{mm}^{(1)} & \mathbf{M}_{ms}^{(2)} \\ & \mathbf{M}_{sm}^{(2)} & \mathbf{M}_{ss}^{(2)} \end{bmatrix} \begin{bmatrix} \Phi_{sm}^{(1)} \\ \Phi_{mm}^{(1)} \\ \Phi_{sm}^{(2)} \end{bmatrix} \Lambda_{mm} \quad (37)$$

where  $\mathbf{K}_{mm} = \mathbf{K}_{mm}^{(1)} + \mathbf{K}_{mm}^{(2)}$  and  $\mathbf{M}_{mm} = \mathbf{M}_{mm}^{(1)} + \mathbf{M}_{mm}^{(2)}$  include degrees of freedom at the interface between the substructures. Since each substructure must be free of the slave degrees of freedom, the first and third rows of Eq. (37) become

$$\begin{aligned} \mathbf{K}_{ss}^{(1)} \Phi_{sm}^{(1)} + \mathbf{K}_{sm}^{(1)} \Phi_{mm}^{(1)} &= (\mathbf{M}_{ss}^{(1)} \Phi_{sm}^{(1)} + \mathbf{M}_{sm}^{(1)} \Phi_{mm}^{(1)}) \Lambda_{mm} \\ \mathbf{K}_{sm}^{(2)} \Phi_{mm}^{(1)} + \mathbf{K}_{ss}^{(2)} \Phi_{sm}^{(2)} &= (\mathbf{M}_{sm}^{(2)} \Phi_{mm}^{(1)} + \mathbf{M}_{ss}^{(2)} \Phi_{sm}^{(2)}) \Lambda_{mm} \end{aligned} \quad (38)$$

The transformation relation between the master and slave DOFs can be found by rearranging Eq. (38) for the slave DOFs as follows

$$\begin{aligned} \Phi_{sm}^{(1)} &= -(\mathbf{K}_{ss}^{(1)})^{-1} \mathbf{K}_{sm}^{(1)} \Phi_{mm}^{(1)} + (\mathbf{K}_{ss}^{(1)})^{-1} (\mathbf{M}_{sm}^{(1)} \Phi_{mm}^{(1)} + \mathbf{M}_{ss}^{(1)} \Phi_{sm}^{(1)}) \Lambda_{mm} \\ \Phi_{sm}^{(2)} &= -(\mathbf{K}_{ss}^{(2)})^{-1} \mathbf{K}_{sm}^{(2)} \Phi_{mm}^{(1)} + (\mathbf{K}_{ss}^{(2)})^{-1} (\mathbf{M}_{sm}^{(2)} \Phi_{mm}^{(1)} + \mathbf{M}_{ss}^{(2)} \Phi_{sm}^{(2)}) \Lambda_{mm} \end{aligned} \quad (39)$$

Based on the definitions of the transformation matrices in each subsystem, the matrices are as follows

$$\begin{aligned} \Phi_{sm}^{(1)} &= \mathbf{t}_{(1)} \Phi_{mm} \\ \Phi_{sm}^{(2)} &= \mathbf{t}_{(2)} \Phi_{mm} \end{aligned} \quad (40)$$

Substituting Eq. (40) into Eq. (39) and arranging the result

$$\begin{aligned} \mathbf{t}_{(1)} &= -(\mathbf{K}_{ss}^{(1)})^{-1} \mathbf{K}_{sm}^{(1)} + (\mathbf{K}_{ss}^{(1)})^{-1} (\mathbf{M}_{sm}^{(1)} + \mathbf{M}_{ss}^{(1)} \mathbf{t}_{(1)}) \Phi_{mm} \Lambda_{mm} \Phi_{mm}^{-1} \\ \mathbf{t}_{(2)} &= -(\mathbf{K}_{ss}^{(2)})^{-1} \mathbf{K}_{sm}^{(2)} + (\mathbf{K}_{ss}^{(2)})^{-1} (\mathbf{M}_{sm}^{(2)} + \mathbf{M}_{ss}^{(2)} \mathbf{t}_{(2)}) \Phi_{mm} \Lambda_{mm} \Phi_{mm}^{-1} \end{aligned} \quad (41)$$

Eq. (41) can be rewritten as

$$\begin{aligned} \mathbf{t}_{(1)} &= \mathbf{T}_G^{(1)} + \mathbf{T}_d^{(1)}; \quad \mathbf{T}_G^{(1)} = -(\mathbf{K}_{ss}^{(1)})^{-1} \mathbf{K}_{sm}^{(1)} \\ \mathbf{T}_d^{(1)} &= (\mathbf{K}_{ss}^{(1)})^{-1} (\mathbf{M}_{sm}^{(1)} + \mathbf{M}_{ss}^{(1)} \mathbf{t}_{(1)}) \Phi_{mm} \Lambda_{mm} \Phi_{mm}^{-1} \\ \mathbf{t}_{(2)} &= \mathbf{T}_G^{(2)} + \mathbf{T}_d^{(2)}; \quad \mathbf{T}_G^{(2)} = -(\mathbf{K}_{ss}^{(2)})^{-1} \mathbf{K}_{sm}^{(2)} \\ \mathbf{T}_d^{(2)} &= (\mathbf{K}_{ss}^{(2)})^{-1} (\mathbf{M}_{sm}^{(2)} + \mathbf{M}_{ss}^{(2)} \mathbf{t}_{(2)}) \Phi_{mm} \Lambda_{mm} \Phi_{mm}^{-1} \end{aligned} \quad (42)$$

In the transformation matrices,  $\mathbf{T}_G$  and  $\mathbf{T}_d$  represent the static and dynamic terms, respectively. Eq. (41) gives us two transformation matrices. These two transformation matrices allow us to reduce the entire assembled system into a simplified one based on only master DOFs as

Robel Weldebrhan Hagos, Geomji Choi, Heejun Sung and Seongmin Chang

$$\begin{bmatrix} \Phi_{sm}^{(1)} \\ \Phi_{mm} \\ \Phi_{sm}^{(2)} \end{bmatrix} = \begin{bmatrix} \mathbf{t}_{(1)} \\ \mathbf{I}_{mm} \\ \mathbf{t}_{(2)} \end{bmatrix} \Phi_{mm} = \mathbf{T} \Phi_{mm} \quad (43)$$

where  $\mathbf{T}$  is the transformation matrix between  $\Phi_{mm}$  and  $\Phi_{sm}$  in the total system, whereas  $\mathbf{I}$  is the unit matrix of size  $m \times m$ . The reduced system matrices can be obtained by substituting Eq. (43) into Eq. (37) and premultiplying  $\mathbf{T}^T$  on the left.

$$\begin{aligned} \mathbf{K}_R &= \mathbf{t}_{(1)}^T \mathbf{K}_{ss}^{(1)} \mathbf{t}_{(1)} + \mathbf{K}_{ms}^{(1)} \mathbf{t}_{(1)} + \mathbf{t}_{(1)}^T \mathbf{K}_{sm}^{(1)} + \mathbf{K}_{mm} + \mathbf{t}_{(2)}^T \mathbf{K}_{sm}^{(2)} + \mathbf{K}_{ms}^{(2)} \mathbf{t}_{(2)} + \mathbf{t}_{(2)}^T \mathbf{K}_{ss}^{(2)} \mathbf{t}_{(2)} \\ \mathbf{M}_R &= \mathbf{t}_{(1)}^T \mathbf{M}_{ss}^{(1)} \mathbf{t}_{(1)} + \mathbf{M}_{ms}^{(1)} \mathbf{t}_{(1)} + \mathbf{t}_{(1)}^T \mathbf{M}_{sm}^{(1)} + \mathbf{M}_{mm} + \mathbf{t}_{(2)}^T \mathbf{M}_{sm}^{(2)} + \mathbf{M}_{ms}^{(2)} \mathbf{t}_{(2)} + \mathbf{t}_{(2)}^T \mathbf{M}_{ss}^{(2)} \mathbf{t}_{(2)} \end{aligned} \quad (44)$$

Based on the equations above, the basic substructuring reduction procedure is derived. However, the transformation matrix for each substructure is not defined entirely. Using Eq. (44), an eigenproblem with  $m$  degrees of freedom can be constructed.

$$\mathbf{K}_R \Phi_{mm} = \mathbf{M}_R \Phi_{mm} \Lambda_{mm} \quad (45)$$

From Eq. (45),  $\Phi_{mm}^{-1} \Lambda_{mm} \Phi_{mm}$  can be expressed as

$$\Phi_{mm}^{-1} \Lambda_{mm} \Phi_{mm} = \mathbf{M}_R^{-1} \mathbf{K}_R \quad (46)$$

Eq. (46) is substituted into Eq. (41) to yield two transformation matrices.

$$\begin{aligned} \mathbf{t}_{(1)} &= -\left(\mathbf{K}_{ss}^{(1)}\right)^{-1} \mathbf{K}_{sm}^{(1)} + \left(\mathbf{K}_{ss}^{(1)}\right)^{-1} \left(\mathbf{M}_{sm}^{(1)} + \mathbf{M}_{ss}^{(1)} \mathbf{t}_{(1)}\right) \mathbf{M}_R^{-1} \mathbf{K}_R \\ \mathbf{t}_{(2)} &= -\left(\mathbf{K}_{ss}^{(2)}\right)^{-1} \mathbf{K}_{sm}^{(2)} + \left(\mathbf{K}_{ss}^{(2)}\right)^{-1} \left(\mathbf{M}_{sm}^{(2)} + \mathbf{M}_{ss}^{(2)} \mathbf{t}_{(2)}\right) \mathbf{M}_R^{-1} \mathbf{K}_R \end{aligned} \quad (47)$$

As the above equations are nonlinear, it is not easy to solve them directly, so they have to be solved iteratively, and this leads to the iterative version of the improved reduction system. However, we are interested in the standard IRS method, so we take the value of the 0th iteration ( $k=1$ ). The iterative forms of Eq. (47) for  $k=1, 2, 3, \dots$ , are expressed as follows

$$\begin{aligned} \mathbf{t}_{(1)}^{(k)} &= -\left(\mathbf{K}_{ss}^{(1)}\right)^{-1} \mathbf{K}_{sm}^{(1)} + \left(\mathbf{K}_{ss}^{(1)}\right)^{-1} \left(\mathbf{M}_{sm}^{(1)} + \mathbf{M}_{ss}^{(1)} \mathbf{t}_{(1)}^{(k-1)}\right) \left(\mathbf{M}_R^{(k-1)}\right)^{-1} \mathbf{K}_R^{(k-1)} \\ \mathbf{t}_{(2)}^{(k)} &= -\left(\mathbf{K}_{ss}^{(2)}\right)^{-1} \mathbf{K}_{sm}^{(2)} + \left(\mathbf{K}_{ss}^{(2)}\right)^{-1} \left(\mathbf{M}_{sm}^{(2)} + \mathbf{M}_{ss}^{(2)} \mathbf{t}_{(2)}^{(k-1)}\right) \left(\mathbf{M}_R^{(k-1)}\right)^{-1} \mathbf{K}_R^{(k-1)} \end{aligned} \quad (48)$$

Initial approximations of the transformation matrices can be calculated as follows

$$\begin{aligned} \mathbf{t}_{(1)}^{(0)} &= \mathbf{T}_G^{(1)} = -\left(\mathbf{K}_{ss}^{(1)}\right)^{-1} \mathbf{K}_{sm}^{(1)} \\ \mathbf{t}_{(2)}^{(0)} &= \mathbf{T}_G^{(2)} = -\left(\mathbf{K}_{ss}^{(2)}\right)^{-1} \mathbf{K}_{sm}^{(2)} \end{aligned} \quad (49)$$

In these matrices, we exclude the dynamic part of Eq. (48), and they are used to construct Guyan reduction matrices in the following manner

*Substructuring-based dynamic reduction method for vibration analysis of periodic composite structures*

$$\begin{aligned}
\mathbf{K}_G &= \begin{bmatrix} (\mathbf{t}_{(1)}^{(0)})^T & \mathbf{I}_{mm} & (\mathbf{t}_{(2)}^{(0)})^T \end{bmatrix} \begin{bmatrix} \mathbf{K}_{ss}^{(1)} & \mathbf{K}_{sm}^{(1)} & \\ \mathbf{K}_{ms}^{(1)} & \mathbf{K}_{mm} & \mathbf{K}_{ms}^{(2)} \\ & \mathbf{K}_{sm}^{(2)} & \mathbf{K}_{ss}^{(2)} \end{bmatrix} \begin{bmatrix} \mathbf{t}_{(1)}^{(0)} \\ \mathbf{I}_{mm} \\ \mathbf{t}_{(2)}^{(0)} \end{bmatrix} \\
&= (\mathbf{t}_{(1)}^{(0)})^T \mathbf{K}_{ss}^{(1)} \mathbf{t}_{(1)}^{(0)} + \mathbf{K}_{ms}^{(1)} \mathbf{t}_{(1)}^{(0)} + (\mathbf{t}_{(1)}^{(0)})^T \mathbf{K}_{sm}^{(1)} + \mathbf{K}_{mm} + (\mathbf{t}_{(2)}^{(0)})^T \mathbf{K}_{sm}^{(2)} \\
&\quad + \mathbf{K}_{ms}^{(2)} \mathbf{t}_{(2)}^{(0)} + (\mathbf{t}_{(2)}^{(0)})^T \mathbf{K}_{ss}^{(2)} \mathbf{t}_{(2)}^{(0)} \\
\mathbf{M}_G &= \begin{bmatrix} (\mathbf{t}_{(1)}^{(0)})^T & \mathbf{I}_{mm} & (\mathbf{t}_{(2)}^{(0)})^T \end{bmatrix} \begin{bmatrix} \mathbf{M}_{ss}^{(1)} & \mathbf{M}_{sm}^{(1)} & \\ \mathbf{M}_{ms}^{(1)} & \mathbf{M}_{mm} & \mathbf{M}_{ms}^{(2)} \\ & \mathbf{M}_{sm}^{(2)} & \mathbf{M}_{ss}^{(2)} \end{bmatrix} \begin{bmatrix} \mathbf{t}_{(1)}^{(0)} \\ \mathbf{I}_{mm} \\ \mathbf{t}_{(2)}^{(0)} \end{bmatrix} \\
&= (\mathbf{t}_{(1)}^{(0)})^T \mathbf{M}_{ss}^{(1)} \mathbf{t}_{(1)}^{(0)} + \mathbf{M}_{ms}^{(1)} \mathbf{t}_{(1)}^{(0)} + (\mathbf{t}_{(1)}^{(0)})^T \mathbf{M}_{sm}^{(1)} + \mathbf{M}_{mm} + (\mathbf{t}_{(2)}^{(0)})^T \mathbf{M}_{sm}^{(2)} \\
&\quad + \mathbf{M}_{ms}^{(2)} \mathbf{t}_{(2)}^{(0)} + (\mathbf{t}_{(2)}^{(0)})^T \mathbf{M}_{ss}^{(2)} \mathbf{t}_{(2)}^{(0)}
\end{aligned} \tag{50}$$

Eq. (50) explains that Guyan reduction matrices are calculated at the substructure level, and then that we combine these reduced matrices to form one reduced system.  $\mathbf{K}_G$  and  $\mathbf{M}_G$  are the initial reduced system matrices of an iterative dynamic condensation as

$$\begin{aligned}
\mathbf{K}_R^{(0)} &= \mathbf{K}_G \\
\mathbf{M}_R^{(0)} &= \mathbf{M}_G
\end{aligned} \tag{51}$$

The initial transformation matrices for  $k=1$  are obtained when Eq. (51) is substituted into Eq. (48) and by using Eq. (49).

$$\begin{aligned}
\mathbf{t}_{(1)}^{(1)} &= -(\mathbf{K}_{ss}^{(1)})^{-1} \mathbf{K}_{sm}^{(1)} + (\mathbf{K}_{ss}^{(1)})^{-1} (\mathbf{M}_{sm}^{(1)} + \mathbf{M}_{ss}^{(1)} \mathbf{t}_{(1)}^{(0)}) (\mathbf{M}_R^{(0)})^{-1} \mathbf{K}_R^{(0)} \\
\mathbf{t}_{(2)}^{(1)} &= -(\mathbf{K}_{ss}^{(2)})^{-1} \mathbf{K}_{sm}^{(2)} + (\mathbf{K}_{ss}^{(2)})^{-1} (\mathbf{M}_{sm}^{(2)} + \mathbf{M}_{ss}^{(2)} \mathbf{t}_{(2)}^{(0)}) (\mathbf{M}_R^{(0)})^{-1} \mathbf{K}_R^{(0)}
\end{aligned} \tag{52}$$

Using Eq. (52), the reduced system matrices for the Standard IRS method becomes

$$\begin{aligned}
\mathbf{K}_R^{(1)} &= \mathbf{K}_{IRS} = \begin{bmatrix} (\mathbf{t}_{(1)}^{(1)})^T & \mathbf{I}_{mm} & (\mathbf{t}_{(2)}^{(1)})^T \end{bmatrix} \begin{bmatrix} \mathbf{K}_{ss}^{(1)} & \mathbf{K}_{sm}^{(1)} & \\ \mathbf{K}_{ms}^{(1)} & \mathbf{K}_{mm} & \mathbf{K}_{ms}^{(2)} \\ & \mathbf{K}_{sm}^{(2)} & \mathbf{K}_{ss}^{(2)} \end{bmatrix} \begin{bmatrix} \mathbf{t}_{(1)}^{(1)} \\ \mathbf{I}_{mm} \\ \mathbf{t}_{(2)}^{(1)} \end{bmatrix} \\
&= (\mathbf{t}_{(1)}^{(1)})^T \mathbf{K}_{ss}^{(1)} \mathbf{t}_{(1)}^{(1)} + \mathbf{K}_{ms}^{(1)} \mathbf{t}_{(1)}^{(1)} + (\mathbf{t}_{(1)}^{(1)})^T \mathbf{K}_{sm}^{(1)} + \mathbf{K}_{mm} + (\mathbf{t}_{(2)}^{(1)})^T \mathbf{K}_{sm}^{(2)} \\
&\quad + \mathbf{K}_{ms}^{(2)} \mathbf{t}_{(2)}^{(1)} + (\mathbf{t}_{(2)}^{(1)})^T \mathbf{K}_{ss}^{(2)} \mathbf{t}_{(2)}^{(1)} \\
\mathbf{M}_R^{(1)} &= \mathbf{M}_{IRS} = \begin{bmatrix} (\mathbf{t}_{(1)}^{(1)})^T & \mathbf{I}_{mm} & (\mathbf{t}_{(2)}^{(1)})^T \end{bmatrix} \begin{bmatrix} \mathbf{M}_{ss}^{(1)} & \mathbf{M}_{sm}^{(1)} & \\ \mathbf{M}_{ms}^{(1)} & \mathbf{M}_{mm} & \mathbf{M}_{ms}^{(2)} \\ & \mathbf{M}_{sm}^{(2)} & \mathbf{M}_{ss}^{(2)} \end{bmatrix} \begin{bmatrix} \mathbf{t}_{(1)}^{(1)} \\ \mathbf{I}_{mm} \\ \mathbf{t}_{(2)}^{(1)} \end{bmatrix} \\
&= (\mathbf{t}_{(1)}^{(1)})^T \mathbf{M}_{ss}^{(1)} \mathbf{t}_{(1)}^{(1)} + \mathbf{M}_{ms}^{(1)} \mathbf{t}_{(1)}^{(1)} + (\mathbf{t}_{(1)}^{(1)})^T \mathbf{M}_{sm}^{(1)} + \mathbf{M}_{mm} + (\mathbf{t}_{(2)}^{(1)})^T \mathbf{M}_{sm}^{(2)} \\
&\quad + \mathbf{M}_{ms}^{(2)} \mathbf{t}_{(2)}^{(1)} + (\mathbf{t}_{(2)}^{(1)})^T \mathbf{M}_{ss}^{(2)} \mathbf{t}_{(2)}^{(1)}
\end{aligned} \tag{53}$$

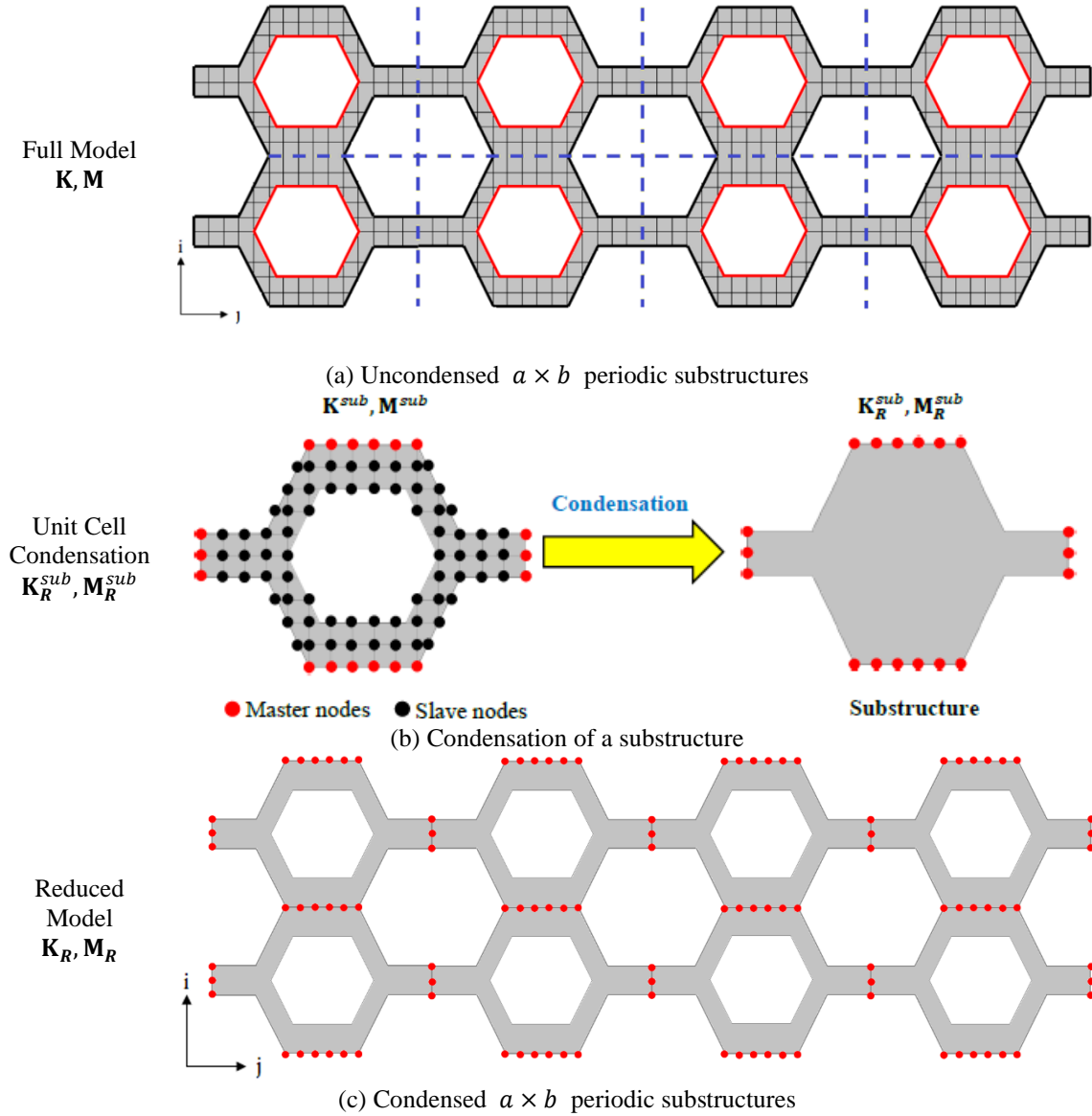


Fig. 2 Condensation of a periodic structure using the proposed method

Solving the generalized eigenproblem of the reduced system, the lowest  $m$  eigenvalues, and their corresponding eigenvectors can be estimated.

$$\mathbf{K}_{IRS} \Phi_{mm} = \mathbf{M}_{IRS} \Phi_{mm} \Lambda_{mm} \quad (54)$$

### 3.3 Substructuring periodic structures using the IRS method

According to Eq. (53), the reduced system matrices are created within each subsystem and

assembled. Whenever a periodic structure exists, all of its substructures share the same structural matrices. Therefore, only one substructure is involved in substructuring.

In Fig. 2(a), a 2D macrostructure is segmented into  $a \times b$  substructures, where  $a$  and  $b$  indicate the number of substructures in the  $i$  and  $j$  direction, respectively. Since finite element models of periodic structures contain repeated geometries, all substructures undergo similar static and dynamic condensations. Condensation of these substructures creates a super-element. Because only the external nodes connected to neighboring elements are retained, the internal shape complexity of the condensed substructure may be lost. Nevertheless, the stiffness and mass matrices of the substructure are reduced considering the uncondensed representation of the substructure. Fig. 2(b) illustrates a typical condensation of a substructure (unit cell). Since all the master and slave DOFs of the original structure contribute to the reduced stiffness and mass matrices ( $\mathbf{K}_R^{sub}$  and  $\mathbf{M}_R^{sub}$ ), no structural information is lost. Compared to the original full stiffness and mass matrices of the substructure ( $\mathbf{K}^{sub}$  and  $\mathbf{M}^{sub}$ ),  $\mathbf{K}_R^{sub}$  and  $\mathbf{M}_R^{sub}$  have a much smaller dimensionality. Thus, the computation becomes more efficient. Through the repeated assembly of the reduced stiffness and mass matrices, the reduced global matrices are obtained using Eqs. (55)-(58). Fig. 2(c) illustrates a condensed periodic structure, and the reduced model has fewer degrees of freedom than the original periodic structure in Fig. 2(a). This results in higher computational efficiency in the macro FEA.

For periodic structures, Eqs. (49)-(53) can be rewritten as follows, respectively.

$$\mathbf{T}_G^{sub} = -(\mathbf{K}_{ss}^{sub})^{-1} \mathbf{K}_{sm}^{sub} \quad (55)$$

$$\mathbf{K}_G = \sum_{i=1}^{a \times b} \mathbf{K}_{mm}^{sub} + \mathbf{K}_{ms}^{sub} \mathbf{T}_G^{sub} + (\mathbf{T}_G^{sub})^T \mathbf{K}_{sm}^{sub} + (\mathbf{T}_G^{sub})^T \mathbf{K}_{ss}^{sub} \mathbf{T}_G^{sub} \quad (56)$$

$$\mathbf{M}_G = \sum_{i=1}^{a \times b} \mathbf{M}_{mm}^{sub} + \mathbf{M}_{ms}^{sub} \mathbf{T}_G^{sub} + (\mathbf{T}_G^{sub})^T \mathbf{M}_{sm}^{sub} + (\mathbf{T}_G^{sub})^T \mathbf{M}_{ss}^{sub} \mathbf{T}_G^{sub}$$

$$\mathbf{T}_{IRS} = \mathbf{T}_G^{sub} + (\mathbf{K}_{ss}^{sub})^{-1} (\mathbf{M}_{sm}^{sub} + \mathbf{M}_{ss}^{sub} \mathbf{T}_G^{sub}) (\mathbf{M}_G)^{-1} \mathbf{K}_G \quad (57)$$

$$\mathbf{K}_R = \mathbf{K}_{IRS} = \sum_{i=1}^{a \times b} \mathbf{K}_{mm}^{sub} + \mathbf{K}_{ms}^{sub} \mathbf{T}_{IRS} + (\mathbf{T}_{IRS})^T \mathbf{K}_{sm}^{sub} + (\mathbf{T}_{IRS})^T \mathbf{K}_{ss}^{sub} \mathbf{T}_{IRS} \quad (58)$$

$$\mathbf{M}_R = \mathbf{M}_{IRS} = \sum_{i=1}^{a \times b} \mathbf{M}_{mm}^{sub} + \mathbf{M}_{ms}^{sub} \mathbf{T}_{IRS} + (\mathbf{T}_{IRS})^T \mathbf{M}_{sm}^{sub} + (\mathbf{T}_{IRS})^T \mathbf{M}_{ss}^{sub} \mathbf{T}_{IRS}$$

#### 4. Numerical implementation

This section presents a computationally efficient implementation of the proposed method. See Table 1 for more information. The reduction process begins with the initialization of the structural mesh and the number of repeated substructures. Following that, the substructures are condensed using the IRS method and assembled to form a reduced macrostructure.

Table 1 Computational procedure of the proposed method

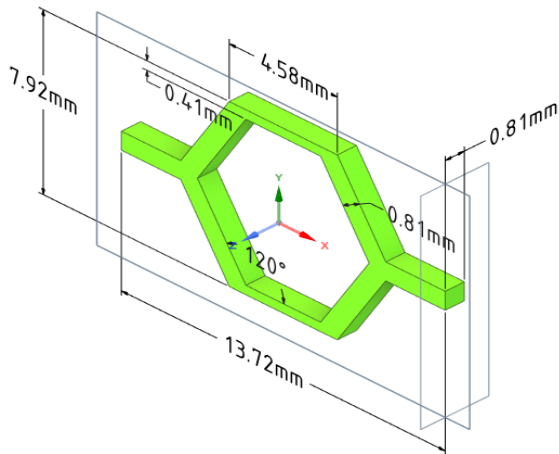
Computational process	Equation numbers
Step 1: Generate the system matrices for the unit cell Generate $\mathbf{K}^{sub}$ and $\mathbf{M}^{sub}$	
Step 2: Choose the master degrees of freedom for the unit cell and partition the system matrices into sub-blocks Set the master ( $m$ ) and slave ( $s$ ) DOFs Generate $\mathbf{K}_{mm}^{sub}, \mathbf{K}_{ms}^{sub}, \mathbf{K}_{sm}^{sub}, \mathbf{K}_{ss}^{sub}$ and $\mathbf{M}_{mm}^{sub}, \mathbf{M}_{ms}^{sub}, \mathbf{M}_{sm}^{sub}, \mathbf{M}_{ss}^{sub}$	22
Step 3: Calculate the Guyan transformation matrix for the unit cell Calculate $\mathbf{T}_G^{sub}$	55
Step 4: Construct the reduced matrices of the Guyan method and assemble them into one Construct $\mathbf{K}_G$ and $\mathbf{M}_G$	56
Step 5: Calculate the IRS transformation matrix Calculate $\mathbf{T}_{IRS}$	57
Step 6: Construct the reduced matrices of the IRS method and assemble them into one Construct $\mathbf{K}_{IRS}$ and $\mathbf{M}_{IRS}$	58
Step 7: Solve for eigenvalue problem of the reduced model	54
Step 8: Calculate the relative eigenfrequency error, $\xi_j$ , using the following formula $\xi_j = \frac{ \bar{\omega}_j - \omega_j }{\omega_j}$ where $\xi_j$ -Relative eigenfrequency error, $\omega_j$ -Modal frequency obtained from the full system, $\bar{\omega}_j$ -Modal frequency calculated from the reduced model	

## 5. Numerical example

In this section, examples are given to illustrate and compare the effectiveness and efficiency of the proposed and homogenization methods. The homogenization was performed using the Material Designer tool from ANSYS®. Material Designer is a component system in ANSYS® Workbench that allows creating composite materials for simulation and homogenized materials of parts made with lattice structures using additive manufacturing. In Material Designer, the RVE is used to represent the microscale structure of the material under consideration. The RVE represents one unit cell for periodic materials, and it repeats itself in all three coordinate directions. Since a single unit cell contains all the information about a material, analyzing its behavior is sufficient. Homogenization begins with modeling the RVE; this requires simplifying the geometry and defining the material properties of the components. Once the geometry has been simplified, it must be meshed to support finite element analysis. Next, the RVE is exposed to several macroscopic load cases, and its response is computed from which homogenized material data are calculated.

As shown in Fig. 3(a), a uniform honeycomb structure with a volume fraction of 19.47% is considered. In Material Designer, we generated the homogenized (effective) material properties, which were then transferred to a new Engineering Data object and applied to the homogenized models. The homogenized models are simple rectangles with no honeycomb structure, but they utilize the material properties calculated using Material Designer. Fig. 3(b)-(d) shows the phase

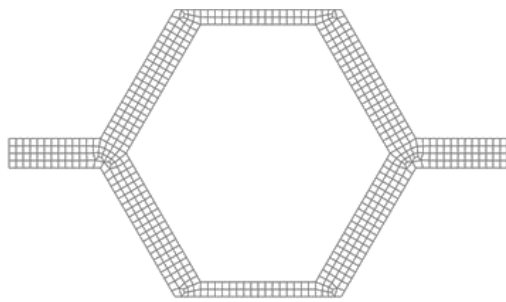
*Substructuring-based dynamic reduction method for vibration analysis of periodic composite structures*



(a) Representative volume element (RVE)

Properties of Outline Row 3: Nylon 12			
	A	B	
1	Property	Value	
2	Material Field Variables	Table	
3	Density	929.99	kg m <sup>-3</sup>
4	Isotropic Elasticity		
5	Derive from	Young's Modulu...	
6	Young's Modulus	1.7E+09	Pa
7	Poisson's Ratio	0.394	
8	Bulk Modulus	2.6729E+09	Pa
9	Shear Modulus	6.0975E+08	Pa

(b) Phase material properties of Nylon 12



(c) 2D meshed geometry of the RVE

Name	Value	Unit
Engineering Constants		
E1	2.5324E+07	Pa
E2	2.5344E+07	Pa
E3	3.3095E+08	Pa
G12	6.0482E+06	Pa
G23	6.5065E+07	Pa
G31	6.5027E+07	Pa
nu12	0.86569	
nu13	0.030149	
nu23	0.030172	
Density		
rho	181.05	kg m <sup>-3</sup>

(d) Homogenized (Effective) material properties

Fig. 3 Honeycomb unit cell and its phase and effective material properties

material properties of the unit cell and the effective material properties obtained from the Material Designer, respectively.

The proposed method was implemented as an independent reduction method using in-house code. The unit cell model was discretized using plane stress quadrilateral elements in ANSYS®; it has 714 nodes, 560 elements, and 1,428 degrees of freedom (2 DOFs per node). The meshed geometry of the unit cell is depicted in Fig. 3(c).

Table 2 shows three honeycomb structures and their homogenized models. The honeycombs are constructed with a periodicity of  $3 \times 3$ ,  $6 \times 6$ , and  $9 \times 9$ , respectively. These structures are fixed at the left edge, and all nodes connected to neighboring elements are designated as master DOFs. In addition, Table 2 shows the number of total and master degrees of freedom and the reduction percentage of each honeycomb using the proposed method. The  $3 \times 3$  honeycomb, for instance, has 360 master DOFs, which are taken into account to construct the reduced system matrices; this makes the final reduced system 2.88% of the global system. Table 3 lists the first ten modal frequencies of the full and reduced models obtained using the proposed method and the first ten modal frequencies of the actual and homogenized models obtained from ANSYS®. Using the

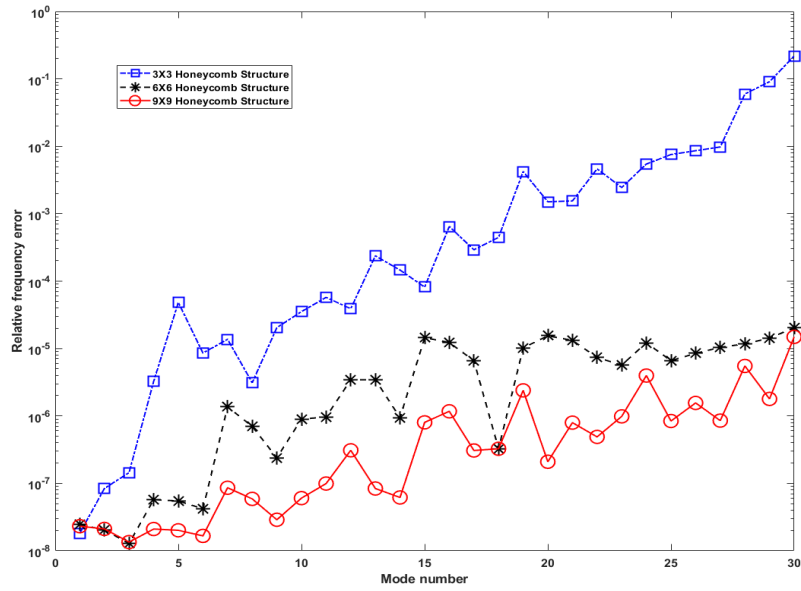
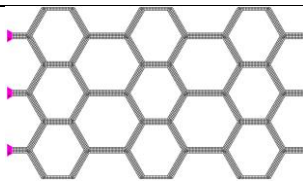
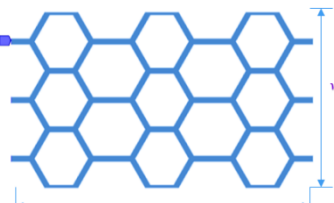

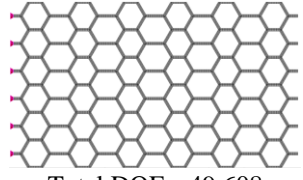
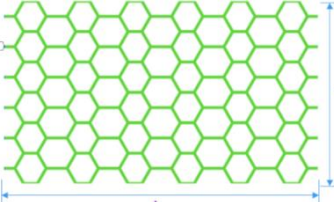


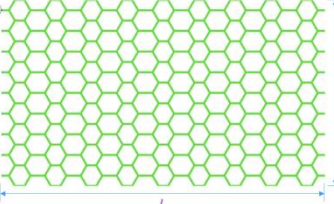



Fig. 4 Relative frequency errors of the proposed method for the honeycomb structures

Table 2 Honeycomb structures and their homogenized models

Periodicity	Proposed Method	ANSYS®	
		Actual Model	Homogenized Model
3 × 3	 Total DOFs=12,492 Reduced DOFs=360 Reduction ratio (%)=2.88%	 $l=41.16$ mm $w=23.76$ mm	 $l=41.16$ mm $w=23.76$ mm
6 × 6	 Total DOFs=49,608 Reduced DOFs=1800 Reduction ratio (%)=3.63%	 $l=82.32$ mm $w=47.52$ mm	 $l=82.32$ mm $w=47.52$ mm
9 × 9	 Total DOFs=11,348 Reduced DOFs=4320 Reduction ratio (%)=3.88%	 $l=123.48$ mm $w=71.28$ mm	 $l=123.48$ mm $w=71.28$ mm



*Substructuring-based dynamic reduction method for vibration analysis of periodic composite structures*

Table 3 The proposed method and ANSYS® results of the first ten modal frequencies (Hz) of the honeycomb structures

Periodicity	Model	Mode										
		1	2	3	4	5	6	7	8	9	10	
3 × 3	In-house-Code Proposed Method	Full	494.4	1959.2	2006.1	3795.9	4382.7	4510.5	4873.4	4947.1	5562.4	6297.8
		Proposed Method	494.4	1959.2	2006.1	3795.9	4382.9	4510.5	4873.5	4947.1	5562.5	6298.0
	Actual	486.1	1928.5	1972.6	3732.3	4299.8	4440.5	4787.6	4864.3	5467.7	6192.8	
	ANSYS® Homogenized	664.5	2170.7	2332.0	4289.0	5088.3	5652.6	6475.0	7027.0	7474.0	7474.2	
	Difference*	0.3100	0.1182	0.1670	0.1388	0.1680	0.2402	0.2996	0.3637	0.3100	0.1875	
6 × 6	In-house-Code Proposed Method	Full	280.3	996.2	1051.8	1957.8	2338.4	2631.1	2776.4	3026.6	3227.2	3472.7
		Proposed Method	280.3	996.2	1051.8	1957.8	2338.4	2631.1	2776.4	3026.6	3227.2	3472.7
	Actual	283.6	1007.1	1063.6	1982.2	2371.2	2668.7	2811.0	3056.7	3265.3	3509.8	
	ANSYS® Homogenized	331.9	1085.1	1165.5	2143.8	2544.2	2825.5	3237.5	3512.3	3736.4	3736.8	
	Difference*	0.1569	0.0746	0.0914	0.0783	0.0704	0.0571	0.1410	0.1387	0.1346	0.0627	
9 × 9	In-house-Code Proposed Method	Full	194.3	666.9	714.3	1317.1	1578.5	1768.1	1942.3	2101.5	2250.9	2336.6
		Proposed Method	194.3	666.9	714.3	1317.1	1578.5	1768.1	1942.3	2101.5	2250.9	2336.6
	Actual	196.4	674.8	721.4	1337.4	1599.0	1786.4	1970.3	2129.2	2275.5	2361.1	
	ANSYS® Homogenized	221.2	723.4	776.9	1429.1	1696.1	1883.6	2158.3	2341.3	2490.9	2491.1	
	Difference*	0.1188	0.0695	0.0741	0.0663	0.0589	0.0530	0.0911	0.0949	0.0904	0.0536	

$$*\text{Difference} = |\omega_{\text{Actual}} - \omega_{\text{Homogenized}}| / \left( \frac{1}{2} (\omega_{\text{Actual}} + \omega_{\text{Homogenized}}) \right)$$

proposed method and ANSYS® actual model, it appears that the natural frequency values are similar, with maximum relative frequency errors of 0.0172, 0.0116, and 0.0104 for the 3 × 3, 6 × 6 and 9 × 9 honeycombs, respectively. As the number of substructures increases, the relative frequency errors decrease. As the periodicity increases from 3 × 3 to 9 × 9, the difference between ANSYS® actual and homogenized models decreases from 0.3100 to 0.1188. In light of this, we can conclude that as we increase the number of substructures in the homogenized model, the results become more accurate and pretty close to the actual model. Fig. 4 compares the relative natural frequencies of the first 30 modes of the three honeycombs generated by the proposed method; as the number of substructures increases, the relative frequency errors decrease. Table 4 shows some selected mode shapes of the three honeycomb structures as obtained using the proposed method and ANSYS®.

## 6. Conclusions

The IRS-based substructuring technique was proposed for accurate and efficient modal analysis of periodic composite structures, and its effectiveness was demonstrated through numerical examples, and it was compared to the homogenization method and found that

- Regardless of the size of the periodic structures under consideration, the proposed method yielded accurate results for low and medium frequency ranges.
- Depending on the number of substructures, the homogenization method had varying levels of

Table 4 Mode shapes of the honeycomb structures as obtained using the proposed method and ANSYS®

Periodicity	Proposed Method	ANSYS®	
		Actual Model	Homogenized Model
3 × 3	Mode 5 Freq. 4382.9 Hz	Mode 5 Freq. 4299.8 Hz	Mode 5 Freq. 5088.3 Hz
	Mode 9 Freq. 5562.5 Hz	Mode 9 Freq. 5467.7 Hz	Mode 9 Freq. 7474.0 Hz
6 × 6	Mode 5 Freq. 2338.4 Hz	Mode 5 Freq. 2371.2 Hz	Mode 5 Freq. 2544.2 Hz
	Mode 10 Freq. 3472.7 Hz	Mode 10 Freq. 3509.8 Hz	Mode 10 Freq. 3736.8 Hz
9 × 9	Mode 4 Freq. 1317.1 Hz	Mode 4 Freq. 1337.4 Hz	Mode 4 Freq. 1429.1 Hz
	Mode 10 Freq. 2336.6 Hz	Mode 10 Freq. 2361.1 Hz	Mode 10 Freq. 2491.1 Hz

accuracy. It became more accurate as the number of substructures increased.

As Geers *et al.* (2010) studied, in the case of the homogenization method, the microscale structures (RVEs) should be significantly smaller than macroscale structures while still being large enough to exhibit the correct macroscale characteristics. In the absence of this assumption, macro and microscales cannot be modeled independently. Moreover, the accuracy of the homogenized solution depends on how well materials, phases, and interfaces are described at the microscale.

## Acknowledgments

This study was supported by the National Research Foundation of Korea (NRF) grant funded by the Korean government (MSIT) (No. 2019R1G1A1005401)

**References**

- Antony, S., Cherouat, A. and Montay, G. (2019), "Hemp fibre woven fabrics/polypropylene based honeycomb sandwich structure for aerospace applications", *Adv. Aircraft Spacecraft Sci.*, **6**(2), 87. <https://doi.org/10.12989/aas.2019.6.2.087>.
- Bendsøe, M.P. and Kikuchi, N. (1988), "Generating optimal topologies in structural design using a homogenization method", *Comput. Method. Appl. Mech. Eng.*, **71**(2), 197-224. [https://doi.org/10.1016/0045-7825\(88\)90086-2](https://doi.org/10.1016/0045-7825(88)90086-2).
- Benjeddou, A. and Guerich, M. (2019), "Free vibration of actual aircraft and spacecraft hexagonal honeycomb sandwich panels: A practical detailed FE approach", *Adv. Aircraft Spacecraft Sci.*, **6**(2), 169. <https://doi.org/10.12989/aas.2019.6.2.169>.
- Benner, P. (2006), "Numerical linear algebra for model reduction in control and simulation", *GAMM-Mitteilungen*, **29**(2), 275-296. <https://doi.org/10.1002/gamm.201490034>.
- Blair, M.A., Camino, T.S. and Dickens, J.M. (1991), "An iterative approach to a reduced mass matrix", *Proceedings of the 8th International Modal Analysis Conference*, Florence, April.
- Cho, M., Yang, S., Chang, S. and Yu, S. (2011), "A study on the prediction of the mechanical properties of nanoparticulate composites using the homogenization method with the effective interface concept", *Int. J. Numer. Method. Eng.*, **85**(12), 1564-1583. <https://doi.org/10.1002/nme.3039>.
- Choi, D., Kim, H. and Cho, M. (2008), "Improvement of substructuring reduction technique for large eigenproblems using an efficient dynamic condensation method", *J. Mech. Sci. Tech.*, **22**(2), 255-268. <https://doi.org/10.1007/s12206-007-1040-7>.
- Craig Jr, R.R. and Bampton, M.C. (1968), "Coupling of substructures for dynamic analyses", *AIAA J.*, **6**(7), 1313-1319. <https://doi.org/10.2514/3.4741>.
- de Klerk, D., Rixen, D.J. and Voormeeren, S.N. (2008), "General framework for dynamic substructuring: History, review and classification of techniques", *AIAA J.*, **46**(5), 1169-1181. <https://doi.org/10.2514/1.33274>.
- Friswell, M.I., Garvey, S.D. and Penny, J.E.T. (1995), "Model reduction using dynamic and iterated IRS techniques", *J. Sound Vib.*, **186**(2), 311-323. <https://doi.org/10.1006/jsvi.1995.0451>.
- Guedes, J. and Kikuchi, N. (1990), "Preprocessing and postprocessing for materials based on the homogenization method with adaptive finite element methods", *Comput. Method. Appl. Mech. Eng.*, **83**(2), 143-198. [https://doi.org/10.1016/0045-7825\(90\)90148-F](https://doi.org/10.1016/0045-7825(90)90148-F).
- Guyan, R.J. (1965), "Reduction of stiffness and mass matrices", *AIAA J.*, **3**(2), 380-380. <https://doi.org/10.2514/3.2874>.
- Hashin, Z. (1983), "Analysis of composite materials: A survey", *J. Appl. Mech. Transac. ASME*, **50**(3), 481-505. <https://doi.org/10.1115/1.3167081>.
- Hill, R. (1963), "Elastic properties of reinforced solids: Some theoretical principles", *J. Mech. Phys. Solid.*, **11**(5), 357-372. [https://doi.org/10.1016/0022-5096\(63\)90036-X](https://doi.org/10.1016/0022-5096(63)90036-X).
- Hollister, S.J. and Kikuchi, N. (1992), "A comparison of homogenization and standard mechanics analyses for periodic porous composites", *Comput. Mech.*, **10**(2), 73-95. <https://doi.org/10.1007/BF00369853>.
- Hurty, W.C. (1960), "Vibrations of structural systems by component mode synthesis", *J. Eng. Mech. Division*, **86**(4), 51-69. <https://doi.org/10.1061/TACEAT.0008073>.
- InSanchez-Palencia, E. and Zaoui, A. (1987), "Homogenization techniques for composite media", *Homogenization Techniques for Composite Media*, 272.
- Irons, B. (1965), "Structural eigenvalue problems-elimination of unwanted variables", *AIAA J.*, **3**(5), 961-962. <https://doi.org/10.2514/3.3027>.
- Kammer, D.C. (1987), "Test-analysis model development using an exact modal reduction", *Int. J. Anal. Exp. Modal Anal.*, **2**(4), 174-179.
- Koutsovasilis, P. and Beitelschmidt, M. (2008), "Comparison of model reduction techniques for large mechanical systems", *Multibody Syst. Dyn.*, **20**(2), 111-128. <https://doi.org/10.1007/s11044-008-9116-4>.
- Li, S. (2008), "Boundary conditions for unit cells from periodic microstructures and their implications",

- Compos. Sci. Tech.*, **68**(9), 1962-1974. <https://doi.org/10.1016/j.compscitech.2007.03.035>.
- Li, S., Jeanmeure, L.A. and Pan, Q. (2015), "A composite material characterisation tool: Unit cells", *J. Eng. Math.*, **95**(1), 279-293. <https://doi.org/10.1007/s10665-014-9776-4>.
- Miller, C.A. (1980), "Dynamic reduction of structural models", *J. Struct. Division*, **106**(10), 2097-2108. <https://doi.org/10.1061/jsdeag.0005546>.
- O'Callahan, J.C. (1988), "System equivalent reduction expansion process (SEREP)", *Proceedings of the 7th International Modal Analysis Conference*, Las Vegas, January.
- O'Callahan, J.C. (1989), "A procedure for an improved reduced system (IRS) model", *Proceedings of the 7th International Modal Analysis Conference*, Las Vegas, February.
- Pourmoayed, A., Fard, K.M. and Roustaa, B. (2021), "Free vibration analysis of sandwich structures reinforced by functionally graded carbon nanotubes", *Compos. Mater. Eng.*, **3**(1), 1-23. <https://doi.org/10.12989/cme.2021.3.1.001>.
- Qu, Z.Q. (2004), *Model Order Reduction Techniques: With Applications in Finite Element Analysis*, Springer. <https://doi.org/10.1007/978-1-4471-3827-3>.
- Rachedi, M.A., Benyoucef, S., Bouhadra, A., Bouiadjra, R.B., Sekkal, M. and Benachour, A. (2020), "Impact of the homogenization models on the thermoelastic response of FG plates on variable elastic foundation", *Geomech. Eng.*, **22**(1), 65-80. <https://doi.org/10.12989/gae.2020.22.1.065>.
- Rixen, D.J. (2004), "A dual Craig-Bampton method for dynamic substructuring", *J. Comput. Appl. Math.*, **168**(1-2), 383-391. <https://doi.org/10.1016/j.cam.2003.12.014>.
- Sayyad, A.S. and Ghugal, Y.M. (2020), "Stress analysis of laminated composite and sandwich cylindrical shells using a generalized shell theory", **2**(2), 103. <https://doi.org/10.12989/cme.2020.2.2.103>.
- Schwarz, H.A. (1890), *Gesammelte Mathematische Abhandlungen*, Springer. <https://doi.org/10.1007/978-3-642-50665-9>.
- Suquet, P.M. (1985), "Elements of homogenization for inelastic solid mechanics, homogenization techniques for composite media", *Lecture Notes in Physics*, **272**, 193.
- van der Seijs, M. (2016), "Experimental dynamic substructuring: Analysis and design strategies for vehicle development", Ph.D. Dissertation of Philosophy, Delft University of Technology (TU Delft), Netherlands.